SIMULATION OF COHERENT OPTICAL TRANSITION RADIATION IN LINAC BASED FREE ELECTRON LASERS

R.B. Fiorito†, A.G. Shkvarunets, J.C. Tobin, University of Maryland, College Park, MD 20742, U.S.A., M. Cornacchia, S. Di Mitri, S. Spampinati, M. Veronese, ELETTRA, Trieste, Italy
H. Loos, J. Wu, LCLS, SLAC, Menlo Park, CA 94025, U.S.A.

Abstract

Recent observations of coherent optical transition radiation (COTR) at LCLS and other laboratories have been recognized as a signature of the micro bunching instability, which affects the longitudinal phase space of the electron beam and ultimately the performance of the Free Electron Laser (FEL). In addition, the COTR emission limits the utility of OTR screens as beam profiling diagnostics. In an effort to understand and predict the extent of COTR emission at diagnostic foil stations and to help specify required instrumentation for new diagnostics, we have independently developed codes at UMD and SLAC-LCLS that use the output from the *ELEGANT* particle tracking code to predict the emission of COTR at specific wavelengths or within a band width chosen by the user. Both COTR codes provide plots of the intensity patterns in the transverse plane, simulating a virtual OTR screen and distinguish between incoherent and coherent emission thus providing an estimate of the micro bunching gain at the observed wavelengths. Since the *ELEGANT* simulation of micro bunching strongly depends on the number of particles, efforts have been carried out to speed up the COTR code analysis. The results of these codes applied to the FERMI@elettra and the LCLS accelerators are presented.

OTR IMAGING CODES

In the OTR codes developed at UMD and LCLS the number of particles and hence computations are significantly reduced by grouping the particles into *M* macro particles (MP). In the UMD code each macro particle has the same radius. In addition the point spread function of a single electron , PSFE = $E_{PE}(\omega,\rho)$, i.e. the Fourier component of the field of a single electron as observed through a lens with diameter D at a distance L from the OTR foil [1], is replaced by the point spread function associated with the macro particle (PSFM). To construct the latter, we assume that each MP is a disc transversely and that the PSFM has the form

$$E_{PM}(\omega,\rho) = S^{-1}\int_S E_{PE}(\omega,\rho-\rho')ds'$$

where S is the area of the MP, ρ and ρ' are transverse radius vectors from the center of the MP to the observation point and to an elemental area within the MP, ds' respectively. Figure1 shows the PSFE and the PSFM for a MP with radius r = 5 μm, the radius used in the UMD simulations presented below. The complex field of the m^{th} MP is given by

$$E_m(\omega,\rho) = E_{PM}(\omega,\rho)\sum_n^m \exp\left(ikz_n/\beta\right)$$

where $\beta = v/c$, v is the velocity of the particle, n is the index of the particle and z_n is the longitudinal position of the n^{th} particle. The superscript m on the sum, which is performed over all N particles, means that the phase of the n^{th} particle conditionally contributes to the sum only if its coordinates fall within the area of the m^{th} MP.

The coherent sum of the fields of all M macro particles is then

$$E(\omega,r) = \sum_{m=1}^{M} E_m(\omega, r-r_m)$$

where r_m is the radius vector of the center of the m^{th} MP. The simulated COTR images presented below are composed from the squared absolute value of this total field.

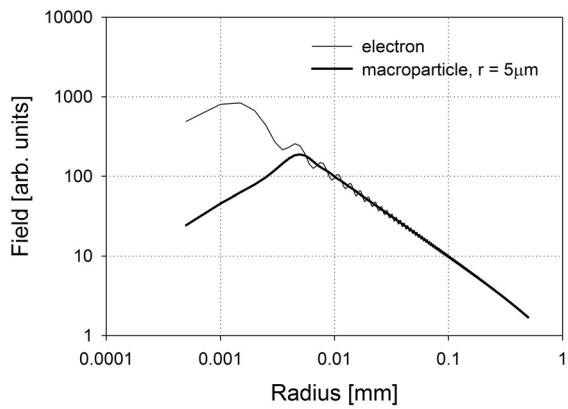

Figure 1: Comparison of PSFE and PSFM of macro particles with radius, r = 5 μm; E = 1167 MeV, λ = 3μm, and the ratio L/D = 1.

The COTR imaging simulation code developed at LCLS was described in [2]. The electric field of the imaged COTR is given by the convolution of the single electron field distribution (the PSFE) with the spectral component of the normalized charge distribution $\rho(r,k)$ at

†corresponding author: rfiorito@umd.edu

the given wave number k. In terms of a Fourier integral the electric field at position r on the imaging screen (assuming unity magnification) can be written as

$$E(\vec{r}) = 2\pi \frac{Ne}{i\pi c} \int_0^{k\theta} d^2\kappa \rho(\kappa, k) \frac{\vec{\kappa} e^{i\vec{\kappa}\vec{r}}}{\kappa^2 + k^2/\gamma^2}$$

with lens acceptance angle θ, number of electrons N, and relativistic factor γ. The spectral components of the charge distribution are in the code generated from the 3D particle locations by binning all the macro-particles into a 2D transverse grid whose grid size is matched to the size of the PSFE. For each cell the phase factors of the particles within this cell are then summed to yield the spectral component of the charge density at this location. The COTR field is then obtained by several fast Fourier transforms.

FERMI@ELETTRA

FERMI@elettra is a fourth generation light source under construction at Sincrotrone Trieste [3]. The project is based upon the conversion and update of the existing 3 GHz, normal conducting Elettra injector linac (now replaced by the Elettra Booster injection system) to a 1.5 GeV machine suitable to drive a seeded Free Electron Laser (FEL) user facility. The FERMI project, now under commissioning, will be completed in two phases, starting from the production of radiation in the 100-20 nm fundamental wavelength range in phase I, down to 4 nm with phase II.

The FERMI@elettra layout is sketched in Fig. 2. The layout reflects intentional choices for the flexible variations of beam parameters as required by the FEL processes and for the preservation of the beam quality that is high peak current, low emittance and low energy spread. The beam delivery system consists of an injector, followed by four linac segments (L1–L4), interleaved by two magnetic chicanes (BC1 and BC2) for a total bunch length compression factor (CF) of up to 10. L1 also includes: a high harmonic cavity module (11.4 GHz) to linearize the beam longitudinal phase space so making the bunch length compression more efficient; a Laser Heater (LH) system for suppression of the microbunching instability (μBI) [4, 5]. The high energy transfer line leads to the single pass undulator chains for the external laser-seeded FEL1 and FEL2; they have single and double cascade schemes, respectively, for High Gain Harmonic Generation (HGHG) [6].

Beam Dynamics

The FERMI@elettra design has crucially relied on computational analysis. A large variety of computer codes was used to establish confidence in achievement of the FERMI@elettra goals, as reported in Table 1. Many

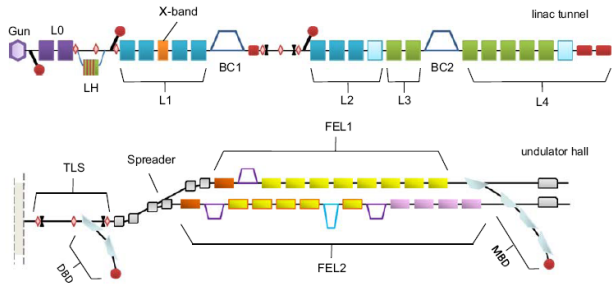

Figure 2: Split schematic of FERMI@elettra: accelerating structures, compressors (BC1, BC2), transfer line (TLS, Spreader), FEL lines and beam dumps (DBD, MBD).

single particle and collective phenomena were numerically simulated. The μBI is probably one of the most important perturbation for FERMI (see [7] and reference therein) because of the harmonic cascade FEL's special sensitivity to the electron beam energy spread [8]. Owing to the combined action of Longitudinal Space Charge (LSC), Coherent Synchrotron Radiation (CSR) and dispersive motion in the compressors, FERMI acts like a huge amplifier of small density and energy modulations [9]. The frequency cutoff of the μBI gain (defined as the ration between the final and initial modulation density amplitude) can be moved toward longer modulation wavelengths, which are transparent to the FEL process, by increasing the uncorrelated energy spread of the electron beam [4]. This is done by the LH system in a very controlled way [10]. However, the final slice energy spread must also not exceed the FEL specifications, as reported in Table 1. Thus, the minimum slice energy spread induced by the LH before compression to suppress the instability has been calculated to be 10keV rms for the single compression scheme [7].

Table 1: Main electron and photon beam parameters of FERMI@elettra FEL1 and FEL2 configuration

Parameter	FEL1	FEL2	Units
Energy	1.2	1.5	GeV
Charge	0.8		nC
Slice Norm. Emitt., rms	1.5		μm rad
Slice.E-Spread, rms	<0.20	<0.15	MeV
Peak Current, flat part	800		A
Bunch Duration, fw	1		ps
Wavelength Range	100 – 20	20 – 4	nm
Pulse Length, rms	≤50	≤50	fs
Peak Power	1 – 5	> 0.3	GW
Repetition Rate	10	50	Hz

Simulation of the μBI was performed with *ELEGANT* [11] starting from shot noise. According to [12], special care was taken to minimize unphysical numerical sampling anomalies introduced by the code when the particle flow is not sufficiently smooth. After that, an

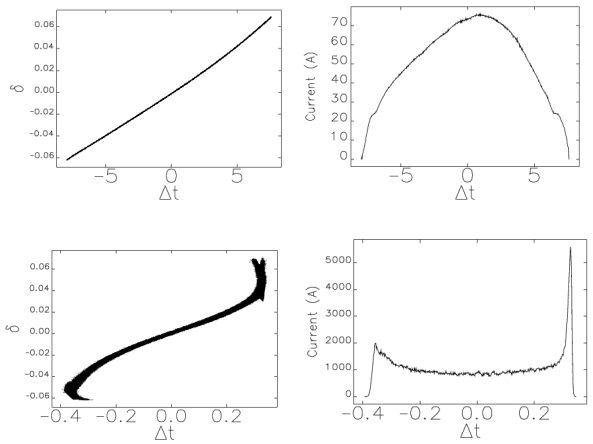

Figure 3: Longitudinal phase space (relative energy deviation vs. bunch duration in ps unit) (left) and current profile (right) of the FERMI@elettra electron bunch before (top row) and after (bottom row) BC1. The bunch length is compressed by a factor 10.

accurate investigation of the final particle distribution pointed out a residual density modulation of 3 μm wavelength. This is consistent with the modulation filtering threshold imposed in the code that allow initial wavelengths longer than 25 μm to propagate through the machine. They are then compressed by a factor 10 as well as the bunch length. Fig. 2 shows the 5 million particle file simulated with *ELEGANT*, before and after the compression in BC1.

OTR CODE Results for FERMI

For the FERMI case studies presented here, the UMD COTR code was used to confirm the presence of microbunching in the above mentioned FERMI particle file and to investigate the efficacy of the LH system in suppressing the instability.

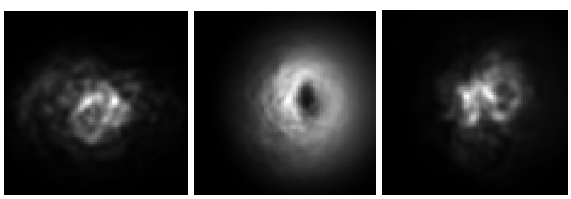

Figure 4: Predicted transverse intensity pattern of CTR observed in the near region for the single compression scheme (CF=10). The 5 million *ELEGANT* particle file on which the CTR simulation was based corresponds to: left, uncompressed beam transported up to BC1; centre, compressed beam transported up to the linac end; right, compressed beam transported up to the linac end with additional heating of 10 keV rms at 100 MeV. The coherent emission at (30) 3 μm is simulated for the (un)compressed beam.

The three plots in Fig. 4 show the transverse intensity pattern of the coherent emission in the near field region; they correspond to three different locations of the electron bunch along the machine and the last one includes the beam heating process.

Using the LCLS code for the Fermi case studies gives similar results as shown in Fig. 5. The imaging optics was assumed to have an acceptance of 75 mrad. For the case at the linac end with no laser heating, an increase of a factor ~40 between coherent and incoherent TR at 3 μm is observed and with laser heating this reduces to ~2.

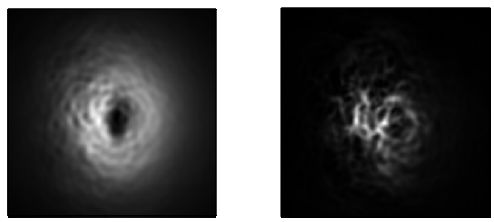

Figure 5: Predicted CTR pattern using the LCLS code corresponding to the Fermi cases at the end of the linac.

LINAC COHERENT LIGHT SOURCE

As mentioned above COTR has been extensively observed at the SLAC LCLS [2]. During the phase III commissioning of LCLS, a Laser Heater has been commissioned [13] which is an inverse free electron laser (IFEL) in which a laser interacts with the electron bunch to imprint energy modulation on the latter at the laser wavelength. This energy modulation is converted into density modulation down stream of the IFEL where dispersive sections exist. The energy and density modulations eventually die away and become pure energy spread due to phase space mixing. COTR at the laser wavelength can be observed in the vicinity of the two dipoles after the undulator. We refer to the COTR thus generated as seeded COTR (SCOTR) in similarity to a seeded FEL [6].

As shown in Fig. 6, the Laser Heater composes of a 4-dipole chicane and a 9-period undulator between the 3rd and the 4th dipole where the laser interacts with the electron bunch. Right after the undulator the electrons pass through two dipoles which provide dispersion

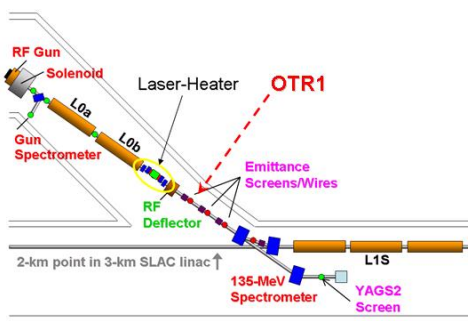

Figure 6: LCLS Laser Heater and screen OTR1 in the LCLS Injector.

function to convert the energy modulation into density modulation. About 1.6 m down stream of the fourth dipole, there is an OTR screen, OTR1 as in Fig. 6. This is a good place to detect the residual density modulation at the laser wavelength by observing the SCOTR spectrum.

Since the dispersion function is fixed in the 3rd and 4th dipole downstream of the density modulation peaks when $R_{56}\delta \approx \lambda / 4$, where R_{56} is the transport matrix element, δ is the laser induced energy modulation amplitude, and λ is the laser wavelength (758 nm). The laser induced energy modulation amplitude δ is proportional to $(E_{Laser})^{1/2}$, where E_{Laser} is the laser energy. Hence, by scanning the laser energy, the density modulation at the laser wavelength will change according, as will the SCOTR on OTR1.

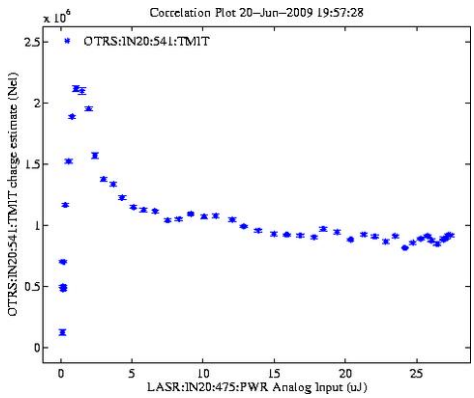

Figure 7: SCOTR on OTR1 screen as a function of the Laser Heater Laser energy.

Figure 7 shows the SCOTR strength on OTR1 as a function of the laser strength. The SCOTR image at a laser energy of about 2 μJ is shown in Fig. 8 with a typical distribution of a partial donut. At this laser energy, the induced energy modulation amplitude is around 15 keV for typical electron beam parameters.

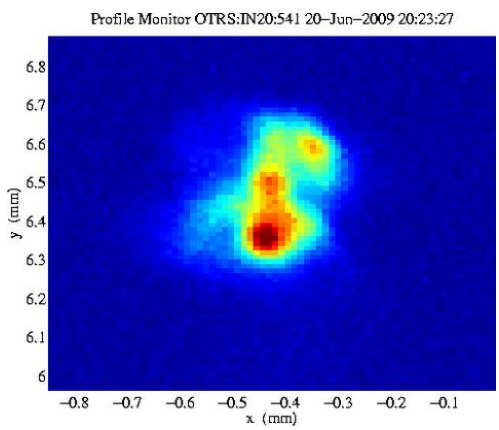

Figure 8: Typical SCOTR image on OTR1 screen showing a partial donut.

The simulation of the SCOTR at LCLS is ongoing. Simulation results using the COTR codes to date do not shown any enhancement compared to the incoherent case because the bunch form factor at the 800 nm seed wavelength in the simulation is at the same level as that of a random distribution of 6 M particles. Figure 9 shows the bunch form factor from an ELEGANT simulation of 6 M particles in the near IR with a laser energy corresponding to an energy modulation of 5 keV.

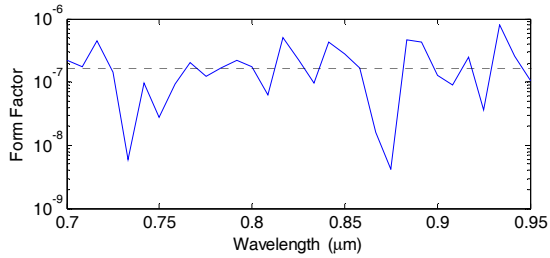

Figure 9: Current spectrum for a laser induced energy modulation amplitude of 5 keV. The dashed line indicates the incoherent limit for 6M particles.

ACKNOWLEDGEMENTS

Sponsors of this research include the US Office of Naval Research and the DOD Joint Technology Office (UMD); and the US Department of Energy under contract DE-AC02-76SF00515 (SLAC-LCLS).

REFERENCES

[1] D. Xiang et al., PRST-AB, **10**, 062801 (2007).
[2] H. Loos et al., FEL08, THBAU01, Gyeongju, Korea; SLAC-PUB 13395.
[3] C.J. Bocchetta et al., "FERMI@elettra CDR",(2007); http://www.elettra.trieste.it/FERMI.
[4] E.L. Saldin et al., NIM A, **483**, 516 (2002).
[5] Z. Huang, K-J. Kim, PRST-AB, **5**, 074401 (2002).
[6] L.H. Yu et al., Science, **289**, 932 (2000).
[7] S. Di Mitri et al., NIM A, 608 (2009) 19-27.
[8] G. De Ninno, E. Allaria, ST/F-TN-09/03 (2009).
[9] M. Venturini et al., PRST-AB, **10**, 104401 (2007).
[10] S. Spampinati et al., FEL07, WEPPH015, Novosibirsk, Russia.
[11] M. Borland et al., NIM A, **483**, 268 (2002).
[12] M. Borland, PRST-AB, **11**, 030701 (2008).
[13] P. Emma et al., PAC09,WE5RFP041,Vancouver, BC